the mode in question were nondegenerate then it would have to transform into plus or minus itself under any point group symmetry operation. Hence there could not be more than two versions of the transition state connected to any given minimum.

Acknowledgment. D.J.W. gratefully acknowledges Lloyd's of London for a Tercentenary Fellowship (1990–91) and the Royal Society for a University Research Fellowship (1991–). R.G.A.B. thanks Clare College, Cambridge, for financial assistance. Some of the SCF results confirm unpublished work performed in 1989 by D.J.W. and Prof. R. F. Stanton using the ACES package.[42] The group theoretical section of this paper benefitted greatly from discussions with Dr. G. K. Sankaran. Our calculations were made possible thanks to grants from the SERC and very generous allowances of disc space by the University of London Computer Centre.

Theoretical Studies of Spin-Forbidden Radiationless Decay in Polyatomic Systems: Insights from Recently Developed Computational Methods

David R. Yarkony

Contribution from the Department of Chemistry, The Johns Hopkins University, Baltimore, Maryland 21218. *Received January 2, 1992*

Abstract: We consider spin-forbidden radiationless decay of a bound electronic state which is metastable owing to a crossing with a dissociative potential energy surface of different spin-multiplicity. The minimum energy point on the spin-allowed surface of intersection of the bound and dissociative potential energy surfaces (the minimum energy crossing point) represents a key bottleneck along the minimum energy dissociation path, and frequently represents the transition state for this process. Thus the characterization of the minimum energy crossing point yields valuable mechanistic insights into this class of reactions, providing information concerning the feasibility of radiationless decay and the likely decomposition products. Traditional approaches for determining this point using multireference CI wave functions are computationally costly. However, a recently introduced algorithm, which uses analytic energy gradients and determines this point directly, that is without prior characterization of the surface of intersection, has reduced considerably the requisite computational effort. This algorithm is used to consider postulated spin-forbidden radiationless decay channels in tetrahedral N_4, $N_4(^1A_1) \rightarrow N_4(^3A'') \rightarrow N_2(X^1\Sigma_g^+) + N_2(A^3\Sigma_u^-)$ and in the methoxy cation, $CH_3O^+(^3A_2) \rightarrow CH_3O^+(^1A') \rightarrow HCO^+(X^1\Sigma^+) + H_2(X^1\Sigma_g^+)$. For the methoxy cation it is shown, using CI expansions as large as 2.5 million configuration state functions, that $\Delta E = 15.4$ kcal/mol, where ΔE is defined as the difference between the energy at minimum energy crossing structure and the energy at the minimum on the bound state potential energy surface. Thus the indicated reaction provides a low energy decomposition pathway. For tetrahedral N_4, ΔE for the indicated process is 28.2 kcal/mol which is half the barrier for the spin-allowed decay channel.

I. Introduction

In this work we consider systems in which the vibrational levels of a bound potential energy surface are rendered metastable by the spin–orbit induced coupling to a dissociative state of different spin-multiplicity. In a phenomenological sense, this process, spin-forbidden predissociation or spin-forbidden radiationless decay, is well understood. However, the computational treatment of this problem in polyatomic systems is particularly challenging. The first task is to establish the dissociation pathway (or pathways) which is (are) energetically accessible to the quasibound molecule. The minimum energy point on the spin-allowed surface of intersection of the two surfaces in question, the minimum energy crossing point, represents a key bottleneck along the minimum energy path[1] and is frequently the transition state for this pathway. Thus the determination of this point (i) provides the barrier for the decomposition pathway, or at least a lower bound if the true transition state lies elsewhere on the bound state surface, and (ii) can, particularly for a late or product channel minimum energy crossing point, establish the products of the radiationless decay process. Clearly then, the determination of this point provides essential information concerning the mechanism and feasibility of spin-forbidden radiationless decay and is a logical starting point for any treatment of this process.

The straightforward procedure that has been used in the past to locate the minimum energy point,[2] the indirect determination of this point, initially determines the crossing surface and then characterizes its minimum. This procedure is computationally costly since for a system with N internal degrees of freedom a crossing surface, or seam, of dimension $N-1$ must be determined and analyzed. Thus the determination of this point represents a computational bottleneck in the study of this class of processes. However, this bottleneck can be avoided. Fletcher[3] has shown that the minimum energy crossing point can be determined by a Lagrange multiplier constrained minimization procedure which determines this point directly, that is, without prior determination of the crossing surface itself. Implementations of this algorithm have been reported initially by Koga and Morokuma[4] based on SCF wave functions and more recently by the present author[5] using MCSCF/CI wave functions.

This work focuses on the use of this methodology to determine the feasibility of proposed spin-forbidden radiationless decay processes. This is the essential first step in a quantitative characterization of a predissociation or radiationless decay rate. The complete description, which is beyond the scope of the present work, requires (i) a more complete knowledge of the relevant potential energy surfaces, (ii) the spin–orbit induced coupling between these potential energy surfaces, and (iii) the solution of

(1) Kato, S.; Jaffe, R. L.; Komornicki, A.; Morokuma, K. *J. Chem. Phys.* **1983**, *78*, 4567.

(2) Alexander, M. H.; Werner, H.-J.; Hemmer, T.; Knowles, P. J. *J. Chem. Phys.* **1990**, *93*, 3307.

(3) Fletcher, R. *Practical Methods of Optimization*; John Wiley: New York, 1981.

(4) Koga, N.; Morokuma, K. *Chem. Phys. Lett.* **1985**, *119*, 371.

(5) Yarkony, D. R. *J. Chem. Phys.* **1990**, *92*, 2457.

0002-7863/92/1514-5406$03.00/0 © 1992 American Chemical Society

a multidimensional electronically nonadiabatic quantum scattering problem.[6-8]

Recently, spin-forbidden radiationless decay has been suggested as a pathway for the decomposition of the methoxy cation, CH_3O^+.[9] This radical cation owes, at least part of, its importance to its radical precursor CH_3O which plays an important role as an intermediate in the combustion of hydrocarbon fuels[10] and atmospheric pollution chemistry.[11] While the cation corresponding to the isomer CH_2OH is readily detectable in photoionization mass spectrometric studies, the observation of CH_3O^+ is more problematical. Recent experiments have detected CD_3O^+ but only observed HCO^+ when CH_3O^+ would have been expected.[9] It has been suggested[9] that this is attributable to the spin-forbidden radiationless decay process

$$CH_3O^+(^3A_2) \rightarrow CH_3O^+(^1A') \rightarrow HCO^+(X^1\Sigma^+) + H_2(X^1\Sigma_g^+) \quad (1.1)$$

While there have been several recent theoretical treatments of the CH_3O^+ cation,[12-15] none address the radiationless decay process in eq 1.1. This work will consider the feasibility of this direct radiationless decay pathway.

The molecule tetrahedral N_4, which has yet to be isolated, has been the object of several previous theoretical studies.[16-22] The most recent studies using correlated wave functions demonstrated that tetrahedral N_4 represents a local minimum (the $^1A_1$ state) on the lowest singlet potential energy surface.[22,23] Recently the possible role of tetrahedral N_4 as a high energy density material in high specific impulse fuels has been raised.[24] A recent study of this system by Lee and Rice[22] estimated the barrier to spin-allowed radiationless decay of $N_4(^1A_1)$ to two N_2 molecules through a C_s symmetry transition state to be approximately 61 kcal/mol. A similar conclusion has also been reached by Lauderdale et al.[23] However, Lee and Rice also found a bound C_s triplet structure on the $^3A''$ potential energy surface, only 13 kcal/mol less stable than $N_4(^1A_1)$. This observation suggests[22,24] that the spin-forbidden radiationless pathway

$$N_4(^1A_1) \rightarrow N_4(^3A'') \rightarrow N_2(X^1\Sigma_g^+) + N_2(A^3\Sigma_u^-) \quad (1.2)$$

may be an important mechanism for the decay of $N_4(^1A_1)$ and might, for example, lead to the predissociation of even the low-lying vibrational levels of N_4. Thus an estimate of the potential for spin-forbidden predissociation of the low-lying vibrational levels of tetrahedral N_4 is essential to a determination of its viability as a high energy density material. In this work the question of spin-forbidden predissociation will be addressed.

Section II briefly reviews the methodology used to determine the minimum energy crossing point and presents the applications to the above noted systems. Section III summarizes and concludes.

II. Theoretical Approach

A. Determining the Minimum Energy Crossing Point. The minimum energy point on a surface of intersection can be determined directly without prior determination of the crossing surface itself, using a Lagrange–Newton[3] procedure[3,4] which minimizes the quantity $L_{IJ}(\mathbf{R},\lambda) = E_I^0(\mathbf{R}) + \lambda\Delta E_{IJ}(\mathbf{R})$, where $\mathbf{R}$ denotes the nuclear coordinates, $\Delta E_{IJ}(\mathbf{R}) = E_I^0(\mathbf{R}) - E_J^0(\mathbf{R})$, $E_I^0(\mathbf{R})$ is the potential energy surface for the Ith state, and λ is a Lagrange multiplier. Minimizing $L_{IJ}(\mathbf{R},\lambda)$ with respect to $\mathbf{R}$ and λ yields the minimum on the potential energy surface $E_I^0(\mathbf{R})$ subject to the constraint that $E_I^0(\mathbf{R}) = E_J^0(\mathbf{R})$. Expanding $L_{IJ}(\mathbf{R},\lambda)$ to second order gives the following system of Lagrange–Newton equations[3-5]

$$\begin{bmatrix} \mathbf{W}^{IJ}(\mathbf{R},\lambda) & \mathbf{g}^{IJ}(\mathbf{R}) \\ \mathbf{g}^{IJ}(\mathbf{R})^\dagger & 0 \end{bmatrix} \begin{bmatrix} \delta\mathbf{R} \\ \delta\lambda \end{bmatrix} = -\begin{bmatrix} \mathbf{g}^I(\mathbf{R}) + \lambda\mathbf{g}^{IJ}(\mathbf{R}) \\ \Delta E_{IJ}(\mathbf{R}) \end{bmatrix} \quad (2.1)$$

where $\delta\mathbf{R} = \mathbf{R}' - \mathbf{R}$, $\delta\lambda = \lambda' - \lambda$, and the energy gradient $g^I(\mathbf{R})$ and energy difference gradient $g^{IJ}(\mathbf{R})$ are given by

$$g_\alpha^I(\mathbf{R}) = \frac{\partial E_I^0(\mathbf{R})}{\partial R_\alpha} \quad (2.2a)$$

$$g_\alpha^{IJ}(\mathbf{R}) = \frac{\partial E_I^0(\mathbf{R})}{\partial R_\alpha} - \frac{\partial E_J^0(\mathbf{R})}{\partial R_\alpha} = \frac{\partial \Delta E_{IJ}(\mathbf{R})}{\partial R_\alpha} \quad (2.2b)$$

and the second derivative matrix, $W^{IJ}(\mathbf{R},\lambda)$, is given by

$$W_{\alpha\beta}^{IJ}(\mathbf{R},\lambda) = \frac{\partial^2 L_{IJ}(\mathbf{R},\lambda)}{\partial R_\alpha \partial R_\beta} = \frac{\partial}{\partial R_\alpha}[g_\beta^I(\mathbf{R}) + \lambda g_\beta^{IJ}(\mathbf{R})] \quad (2.3)$$

$W_{\alpha\beta}^{IJ}(\mathbf{R},\lambda)$ can be determined using a forward or a centered difference of $g_\beta^I + \lambda g_\beta^{IJ}$, that is:

$$W_{\alpha\beta}^{IJ}(\mathbf{R},\lambda) = \{[g_\beta^I(\mathbf{R} + \epsilon\mathbf{I}^\alpha) + \lambda g_\beta^{IJ}(\mathbf{R} + \epsilon\mathbf{I}^\alpha)] - [g_\beta^I(\mathbf{R}) + \lambda g_\beta^{IJ}(\mathbf{R})]\}/\epsilon \quad (2.4a)$$

or

$$W_{\alpha\beta}^{IJ}(\mathbf{R},\lambda) = \{[g_\beta^I(\mathbf{R} + \epsilon\mathbf{I}^\alpha) + \lambda g_\beta^{IJ}(\mathbf{R} + \epsilon\mathbf{I}^\alpha)] - [g_\beta^I(\mathbf{R} - \epsilon\mathbf{I}^\alpha) + \lambda g_\beta^{IJ}(\mathbf{R} - \epsilon\mathbf{I}^\alpha)]\}/2\epsilon \quad (2.4b)$$

where $\mathbf{I}^\alpha$ is a unit vector along the direction R_α. The gradient and energy difference gradient are evaluated, without recourse to divided difference differentiation, using analytic gradient techniques.[5] It is important to observe that, because analytic gradient techniques are used to evaluate the right-hand side of eq 2.1, *it is not necessary to limit the number of nuclear degrees of freedom considered in that equation.*

The wave functions $\Psi^0(I)$ must provide reliable descriptions of both potential energy surfaces $E^0(I)$ and $E^0(J)$. We use $\Psi^0(I) \equiv \Psi_I^0(\mathbf{r};\mathbf{R})$ and $E^0(I) \equiv E_I^0(\mathbf{R})$ when the coordinate dependence of the wave function or energy can be suppressed. The crossing seam will frequently occur in regions of nuclear coordinate space for which bonds are significantly stretched. Thus a multireference description of the wave functions is desirable. In addition, it will ultimately be necessary to determine the intersurface coupling, the spin–orbit matrix elements, between the states in question. As the full microscopic spin–orbit interaction contains both one- and two-electron operators, the spin–orbit and spin–other-orbit terms, respectively,[25,26] the description of both states in terms of

(6) Child, M. S. *Molecular Collision Theory*; Plenum Press: New York, 1974.
(7) Child, M. S.; Lefebvre, R. *Mol. Phys.* **1977**, *34*, 979.
(8) Villarreal, P.; Miret-Artes, S.; Roncero, O.; Delgado-Barrio, G.; Beswick, J. A.; Halberstadt, N.; Coalson, R. D. *J. Chem. Phys.* **1991**, *94*, 4230.
(9) Ruscic, B.; Berkowitz, J. *J. Chem. Phys.* **1991**, *95*, 4033.
(10) Demerjian, K. L.; Kerr, J. A.; Calvert, J. G. *Adv. Environ. Sci. Technol.* **1974**, *4*, 1.
(11) Heicklen, J. *Atmospheric Chemistry*; Academic Press: New York, 1976.
(12) Whangbo, M.; Wolfe, S.; Bernardi, F. *Can. J. Chem.* **1975**, *53*, 3040.
(13) Larrieu, C.; Dargelos, A.; Chaillet, M. *Nouv. J. Chim.* **1981**, *5*, 365.
(14) Bouma, W. J.; Nobes, R. H.; Radom, L. *Org. Mass Spectrom.* **1982**, *17*, 315.
(15) Curtiss, L. A.; Kock, L. D.; Pople, J. A. *J. Chem. Phys.* **1991**, *95*, 4040.
(16) Guest, M. F.; Hillier, I. H.; Saunders, V. R. *J. Chem. Soc., Faraday Trans. 2* **1972**, *68*, 2070.
(17) Wright, J. S. *J. Am. Chem. Soc.* **1974**, *96*, 4753.
(18) Venanzi, T. J.; Schulman, J. M. *Mol. Phys.* **1975**, *30*, 281.
(19) Trinquier, G.; Malrieu, J.; Daudley, J. *Chem. Phys. Lett.* **1981**, *80*, 552.
(20) Novaro, O.; Castillo, S. *Int. J. Quantum Chem.* **1984**, *26*, 411.
(21) Francl, M. M.; Chesick, J. P. *J. Phys. Chem.* **1990**, *94*, 526.
(22) Lee, T. J.; Rice, J. E. *J. Chem. Phys.* **1991**, *94*, 1215.
(23) Lauderdale, W. J.; Stanton, J. F.; Bartlett, R. J. *J. Phys. Chem.* **1992**, *96*, 1173.
(24) Lauderdale, W. J.; Myers, M. J.; Bernholdt, D. E.; Stanton, J. F.; Bartlett, R. J. The Search for Tetrahedral N_4. In *Proceedings of the High Energy Density Materials Contractors Conference*; AFOSR: Washington, DC, 1990.
(25) Bethe, H. A.; Salpeter, E. E. *Quantum Mechanics of One and Two Electron Atoms*; Plenum/Rosetta: New York, 1977.
(26) Langhoff, S. R.; Kern, C. W. Molecular Fine Structure. In *Modern Theoretical Chemistry*; Schaefer, H. F., Ed.; Plenum: New York, 1977; p 381.

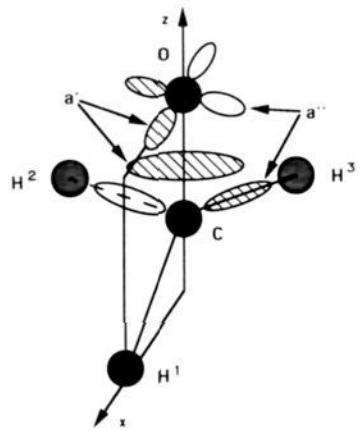

Figure 1. CH_3O^+: representative C_s symmetry structure and orbitals involved in the concerted spin-forbidden decomposition of CH_3O^+. Two a′ contributions to the 7a′ orbital, an H^2–H^3 bonding orbital and an oxygen 2p orbital, and two a″ contributions to the 2a″ orbital, a C–H^i, i = 2, 3, bonding orbital and an oxygen 2p orbital, are shown. Orbital lobes with hatching have positive phase; those with no hatching have negative phase.

a common orthonormal molecular orbital basis is indicated. Thus in our present implementation of the above procedure the wave functions are flexible multireference CI wave functions based on molecular orbitals developed from a state averaged MCSCF (SA-MCSCF)[27-30] procedure. In this work the solution of eq 2.1 in configuration state function (CSF)[31] spaces of between 200 000 and 2 500 000 terms will be presented.

B. Spin–Orbit Interactions. It will emerge that for both systems treated in this work a $^1A'$ and a $^3A''$ potential energy surface that are coupled by the spin–orbit interaction will be considered. Although interstate coupling is not central to this work, it is appropriate to demonstrate that this interaction is not negligible in the vicinity of the minimum energy crossing point. The evaluation of the matrix elements of the full microscopic spin–orbit operator[26] (the spin–orbit and spin–other orbit contributions) in the large CSF spaces used in this work is accomplished using an algorithm[32] based on the symbolic matrix element method.[33]

There are in principle three spin–orbit matrix elements connecting the nonrelativistic wave functions $\Psi[^3A''(M_s)]$, M_s = 1, 0, −1, and $\Psi[^1A'(0)]$. However, in the C_s point group, which as discussed below is sufficient for the present purposes, only two are unique. In particular, defining[34]

$$\Psi_{1A'}(^1A') = \Psi[^1A'(0)] \quad (2.5a)$$

$$\Psi_{1A'}(^3A'') = i\Psi[^3A''(0)] \quad (2.5b)$$

$$\Psi_{2A'}(^3A'') = i\{\Psi[^3A''(1)] - \Psi[^3A''(-1)]\}/\sqrt{2} \quad (2.5c)$$

$$\Psi_{1A''}(^3A'') = i\{\Psi[^3A''(1)] + \Psi[^3A''(-1)]\}/\sqrt{2} \quad (2.5d)$$

we have

$$H_\perp^{so} = \langle\Psi_{2A'}(^3A'')|H^{so}|\Psi_{1A'}(^1A')\rangle \quad (2.6a)$$

$$H_\parallel^{so} = \langle\Psi_{1A'}(^3A'')|H^{so}|\Psi_{1A'}(^1A')\rangle \quad (2.6b)$$

while

$$\langle\Psi_{1A''}(^3A'')|H^{so}|\Psi_{1A'}(^1A')\rangle = 0 \quad (2.6c)$$

by symmetry. The triplet wave functions are chosen to be purely imaginary-valued so that the spin–orbit matrix elements will be real-valued. The values of $H_\perp^{so}$ and $H_\parallel^{so}$ will be reported at the minimum energy crossing points determined in this study.

Table I. CH_3O^+: Energies and Geometries of Minima Obtained from SOCI Wave Functions[a]

structure	MIN-($^3A_2$)(DZP)	MIN-($^3A_2$)(TZ2P)	MEX(DZP)	MEX(TZ2P)
R(C–O)	1.341	1.330	1.276	1.265
R(C–H^1)	1.116	1.112	1.096	1.089
R(C–H^{23})	1.116	1.112	1.170	1.167
R(H^2–H^3)	1.842	1.835	1.375	1.393
∠OCH^1	107.7	107.7	122.0	121.7
∠OCH^{23}	107.7	107.7	108.6	108.4
$E(^3A_2)$	−114.316 346	−114.364 976	−114.289 511	−114.340 387
$E(^1A')$			−114.289 511	−114.340 387
ΔE	0	0	16.8	15.4

[a] Distances in angstroms, angles in degrees, total energies in atomic units; $\Delta E \equiv E(\text{MEX}) - E(^3A_2)$ in kcal/mol. For comparison at MIN($^3A_2$) R(C–O) = 1.309 Å, R(H–C) = 1.119 Å, ∠OCH = 108.3° (from ref 15), and at the equilibrium structure for $HCO^+(X^1\Sigma^+)$ R(CO) = 1.105 Å, R(HC) = 1.086–1.098 Å, (from refs 55 and 56).

C. Spin-Forbidden Decomposition of CH_3O^+/CD_3O^+. The quasibound ground electronic state of CH_3O^+ is the 1^3A_2 state (C_{3v} symmetry). Since we are concerned with the possibility of the concerted decomposition given in eq 1.1, it is computationally convenient to assume a plane of symmetry, containing only the incipient HCO^+ moiety, in the calculations reported here (see Figure 1). In C_s symmetry this state has $^3A''$ symmetry. The dissociation channel of interest corresponds to $HCO^+(X^1\Sigma^+)$ + $H_2(X^1\Sigma_g^+)$ and thus is the $1^1A'$ state in C_s symmetry. The restriction to C_s symmetry is considered further below.

Two contracted Gaussian basis sets were used: (i) a standard Dunning–Huzinaga double-zeta polarization (DZP) basis[35] and (ii) a more extended contracted Gaussian basis set that is of better than triple zeta double polarization quality and is denoted TZ2P. This latter basis is (6s4p2d) on carbon and oxygen based on the (11s7p) contracted bases of van Duijneveldt[36] with two d functions following Dunning,[37] and a 4s2p basis on hydrogen.[34]

The description of the $^3A''$ and $^1A'$ wave functions is based on the following partitioning of the molecular orbitals (1a′–3a′)^6-{4a′–8a′,1a″–2a″},[10] where the core orbitals and active orbitals are denoted by ( ) and {} brackets, respectively. The core orbitals represent the carbon and oxygen 1s orbitals and the oxygen 2s orbital. The active orbitals include the three C–H, and one C–O, σ bonds, the two oxygen $2p_\pi$ orbitals, and an additional a′ function to help describe orbital relaxation among the nominally similar orbitals in the $^3A''$ and $^1A'$ states. The remaining orbitals are virtual orbitals with the exception of the three orbitals with the largest orbital energies which are the truncated orbitals. The CI wave functions were determined in second-order CSF spaces, that is, all CSFs obtained from the following distributions of electrons in the (core, active, virtual, truncated) orbitals (6, 10 − i, i, 0), for i = 0, 1, 2. These second-order spaces consist of (528 762; 2,690 880) CSFs for the $^3A''$ space and (320 068; 1 619 244) CSFs for the $^1A'$ space for the (DZP; TZ2P) bases. The molecular orbitals were determined from a complete active space (CAS)[38-40] SA-MCSCF procedure based on the electron distribution (1a′–4a′)^8{5a′–8a′,1a″–2a″}^{8} in which one state of $^3A''$ symmetry and one of $^1A'$ symmetry were averaged with equal weights.

Table I reports the solution of eq 2.1 using the DZP and TZ2P bases, labeled MEX($^3A''$–$^1A'$)(DZP) and MEX($^3A''$–$^1A'$)(TZ2P), respectively, and compares it with the equilibrium structure for the $^3A_2$ state obtained at the same level of treatment and labeled MIN($^3A_2$)(DZP) and MIN($^3A_2$)(TZ2P). The energies reported

(27) Werner, H.; Meyer, W. *J. Chem. Phys.* **1981**, *74*, 5794.
(28) Hinze, J. *J. Chem. Phys.* **1973**, *59*, 6424.
(29) Lengsfield, B. H. *J. Chem. Phys.* **1982**, *77*, 4073.
(30) Diffenderfer, R. N.; Yarkony, D. R. *J. Phys. Chem.* **1982**, *86*, 5098.
(31) Shavitt, I. The Method of Configuration Interaction. In *Modern Theoretical Chemistry*; Schaefer, H. F., Ed.; Plenum Press: New York, 1976; p 189.
(32) Yarkony, D. R. *J. Chem. Phys.* **1986**, *84*, 2075.
(33) Liu, B.; Yoshimine, M. *J. Chem. Phys.* **1981**, *74*, 612.
(34) Yarkony, D. R. *J. Chem. Phys.* **1990**, *92*, 320.
(35) Dunning, T. H. *J. Chem. Phys.* **1971**, *55*, 716.
(36) van Duijneveldt, F. B. Technical Report RJ945; IBM Research Lab: San Jose, CA, 1971.
(37) Dunning, T. H., Jr. *J. Chem. Phys.* **1989**, *90*, 1007.
(38) Roos, B. O.; Taylor, P. R.; Siegbahn, P. E. M. *Chem. Phys.* **1980**, *48*, 157.
(39) Roos, B. O. *Int. J. Quantum Chem. Symp.* **1980**, *14*, 175.
(40) Siegbahn, P.; Heiberg, A.; Roos, B.; Levy, B. *Phys. Scr.* **1980**, *21*, 323.

in Table I illustrate the gratifying result that our algorithm, for solving eq 2.1 routinely produces energies which are degenerate to less than 2×10^{-6} au. For the DZP calculations the $\mathbf{W}^{IJ}$ matrix in eq 2.1 was determined by forward difference differentiation using eq 2.4a. However, because of the expense involved in determining the CI wave functions using the TZ2P basis, the DZP $\mathbf{W}^{IJ}$ matrix was used for the TZ2P calculations and the iterative solution of eq 2.1 was halted when the norm of the right-hand side was less than 0.1×10^{-2}.

From Table I the results from the DZP and TZ2P treatments are seen to be quite similar. An analysis of the geometrical structure and local topology of the potential energy surfaces at MEX(^{3}A″–^{1}A′) provides insights into the reaction mechanism. The principal structural difference between MIN($^3A_2$) and MEX(^{3}A″–^{1}A′) is R(H^2–H^3) which is almost 0.5 Å shorter for MEX(^{3}A″–^{1}A′). In addition, R(H^1–H^2) = R(H^1–H^3) increases from 1.84 Å at MIN($^3A_2$) to 1.93 Å MEX(^{3}A″–^{1}A′). These changes suggest the incipient formation of an H_2 bond leading to the dissociation channel in eq 1.1. An examination of the energy gradients on the ^{1}A′ potential energy surface at MEX(^{3}A″–^{1}A′) serves to confirm this hypothesis. The "downhill" direction on this surface shortens R(H^2–H^3), R(C–O), and R(C–H^1) while increasing R(C–H^2) = R(C–H^3), thus moving in the direction of the products H_2 and HCO^+ (see footnote in Table I for the equilibrium structure of HCO^+). The downhill direction on the ^{3}A′ surface has the opposite effect on the indicated bond distances.

Additional aspects of the mechanism of the concerted decomposition can be obtained by considering the differences in electronic structure between the ^{3}A″ and ^{1}A′ states at MEX(^{3}A″–^{1}A′). These differences are explained using Figure 1. At MEX(^{3}A″–^{1}A′) the singlet wave function, with principal electron configuration

$$1a'^2...7a'^21a''^2 \tag{2.7a}$$

differs from the triplet wave function, with principal electron configuration

$$1a'^2...6a'^27a'1a''^22a'' \tag{2.7b}$$

by the promotion 2a″ → 7a′. The principal contributors to the 7a′ and 2a″ orbitals are depicted in Figure 1. From this figure it is seen that this promotion corresponds to the transfer of an electron from an a″ orbital that is C–H^i, (i = 2, 3) bonding to an a′ orbital that is H^2–H^3 bonding, while the intra-oxygen portion of the orbital change corresponds to the excitation from the $^3A_2$ state to the ^{1}E state of unperturbed CH_3O^+. Thus the singlet state at this geometry represents a linear combination of the excited ^{1}E state of CH_3O^+ and a state dissociating to $HCO^+ + H_2$. These observations are consistent with the above-noted changes in bond distances.

Using the TZ2P basis results, $\Delta E \equiv E$[MEX(^{3}A″–^{1}A′)] – E[MIN($^3A_2$)] = 15.4 kcal/mol (see Table I). Thus reaction 1.1 clearly provides a low energy decay pathway for CH_3O^+/CD_3O^+. As noted in the Introduction, a precise determination of the lifetimes of the individual vibrational levels requires more complete analysis of the bound ^{3}A″ and dissociative ^{1}A′ potential energy surfaces which will be the object of a future study. However, it is important to note that the vibrational levels with energies less than E[MEX(^{3}A″–^{1}A′)] can predissociate via quantum mechanical tunnelling.[41-43] Recently we have treated an analogous process, the radiationless decay of the c$^1\Pi$ state in NH/ND which is predissociated by a curve crossing with the repulsive $1^5\Sigma^-$ state. There it was found that the v = 0 level in NH, which is significantly below the curve crossing, was appreciably predissociated, whereas the v = 0 level in ND was not.[42]

These observations are consistent with the recent CD_3O^+/CH_3O^+ photoionization experiments of Ruscic and Berkowitz[9] that were able to observe CD_3O^+ but detected only HCO^+ when CH_3O was photoionized. A more detailed comparison with this experiment requires a careful analysis of the excitation process to quantify the vibrational levels of CH_3O^+ initially prepared together with the above-noted analysis of the lifetimes of the individual vibrational levels.

The constraint of C_s symmetry was considered using the TZ2P basis. The C_s symmetry SA-MCSCF/CI expansions used above would have been prohibitively large in C_1 (no spatial) symmetry. Instead, the ^{3}A and ^{1}A wave functions were described at the single and double excitation CI(SDCI) level using as reference electron configurations the C_1 equivalents of electron configuration 2.7b for the ^{3}A state, and electron configurations 2.7a and $1a'^2...6a'^21a''^22a''^2$ for the ^{1}A state. The resulting CSF expansions are of dimension (430 355; 227 706) for the (^{3}A; ^{1}A) states. The molecule was distorted from C_s symmetry at MEX(^{3}A″–^{1}A′) and eq 2.1 resolved. Only an insignificant deviation from C_s symmetry was found in the optimized structure. Thus we conclude that the spin-forbidden radiationless decay results in the concerted or direct elimination of H_2 indicated in reaction 1.1.

The spin-orbit interactions $H_\perp^{so}$ and $H_\parallel^{so}$ were determined at MEX(^{3}A″–^{1}A′) using the DZP basis and were found to be, $H_\perp^{so}$ = 11.3 cm^{-1} and $H_\parallel^{so}$ = 66.4 cm^{-1}. Using these data, an estimate of the probability for a singlet–triplet intersystem crossing can be obtained from an approximate Landau–Zener model.[44-46] While no substitute for a rigorous dynamical treatment, this model estimates the probability for a single pass intersurface transition as $P = 1 - P^{LZ}$, where

$$P^{LZ} = \exp[-(\pi/4)\xi] \tag{2.8a}$$

$$\xi = \frac{8|\langle \Psi_I^0 | H^{so} | \Psi_J^0 \rangle|^2}{\sum_\alpha g_\alpha^{IJ} \cdot \mathbf{v}_\alpha} \tag{2.8b}$$

and $\mathbf{v}$ is an appropriate nuclear velocity vector. Equation 2.8 illustrates how the intersystem crossing probability depends on the spin–orbit coupling and the local topology of the potential energy surfaces (through the energy difference gradient). Note that the energy difference gradient $\mathbf{g}^{IJ}$ required in expression 2.8b is obtained directly from the procedure used to locate the minimum energy crossing point (see eqs 2.1–2.2). Using eq 2.8, with a translational energy of 1500 cm^{-1} directed along an approximate dissociation coordinate, it is estimated that vibrational states with energies above the minimum energy crossing will intersystem cross within 1000 vibrational periods, that is, 1000 passes through the intersurface crossing. Decay rates for the predissociated levels, that is, levels below the minimum energy crossing point energy, cannot be considered in this approximate manner and require a more complete treatment of the decay process.

This Landau–Zener-based, time-dependent interpretation of the radiationless decay process is similar in spirit to the intermediate complex model[47,48] used to explain the efficiency of spin-forbidden quenching reactions such as

$$O(^1D) + N_2(X^1\Sigma_g^+) \rightarrow N_2O \rightarrow O(^3P) + N_2(X^1\Sigma_g^+)$$

$$O(^1D) + CO(X^1\Sigma^+) \rightarrow CO_2 \rightarrow O(^3P) + CO(X^1\Sigma^+)$$

which are of importance in atmospheric chemistry[47] and the spin-forbidden reaction

$$CH(X^2\Pi) + N_2(X^1\Sigma_g^+) \rightarrow HCN_2 \rightarrow HCN(X^1\Sigma^+) + N(^4S)$$

which is of importance in combustion chemistry.[49-52] Because

(41) Lee, T. J.; Handy, N. C.; Rice, J. E.; Scheiner, A. C.; Schaefer, H. F. *J. Chem. Phys.* **1986**, *85*, 3930.
(42) Parlant, G.; Dagdigian, P. J.; Yarkony, D. R. *J. Chem. Phys.* **1991**, *94*, 2364.
(43) Parlant, G.; Senekowitsch, J.; ONeil, S. V.; Yarkony, D. R. *J. Chem. Phys.* **1991**, *94*, 7208.
(44) Nikitin, E. E. In *Chemische Elementarprozesse*; Hartmann, H., Ed.; Springer: Berlin, 1968.
(45) Nikitin, E. E. *Adv. Quantum Chem.* **1970**, *5*, 135.
(46) Desouter-Lecomte, M.; Lorquet, J. C. *J. Chem. Phys.* **1979**, *71*, 4391.
(47) Tully, J. C. *J. Chem. Phys.* **1974**, *61*, 61.
(48) Zahr, G. E.; Preston, R. K.; Miller, W. H. *J. Chem. Phys.* **1975**, *62*, 1127.
(49) Fenimore, C. P. 13th Symposium (International) on Combustion; The Combustion Institute: Pittsburgh, PA, 1971.
(50) Blauwens, J.; Smets, B.; Peeters, J. 16th Symposium (International) on Combustion; The Combustion Institute: Pittsburgh, PA, 1977.

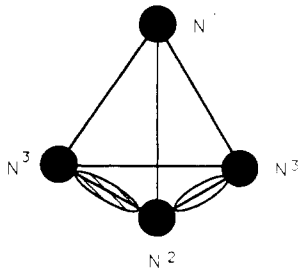

Figure 2. N_4: representative C_s symmetry structure and 4a″ orbital. Orbital lobes with hatching have positive phase, those with no hatching have negative phase.

of the existence of an intermediate complex, attributable to local minimum on the entrance channel potential energy surface, these reactions can occur despite a small probability for a single pass intersystem crossing by repeatedly traversing the crossing surface. The minimum energy crossing point methodology used here can also play a key role in the elucidation of the electronic structure aspects of these reactions.[53,54]

D. Spin-Forbidden Decomposition of Tetrahedral N_4. As noted in the Introduction, the barrier to spin-allowed decay of tetrahedral N_4 is quite large, approximately 61 kcal/mol. This subsection is concerned with possibility that spin-forbidden radiationless decay induced by spin–orbit coupling to the $1^3A''$ state can provide a lower energy pathway for radiationless decay of tetrahedral N_4. C_s symmetry notation corresponding to the geometrical arrangement in Figure 2 will be used since Lee and Rice[22] have shown that both the transition state for spin-allowed radiationless decay and the local minimum on the lowest triplet potential energy surface have this symmetry.[22] It emerged that the minimum energy crossing point indeed also has this symmetry. However, since this need not have been the case, the final calculations reported in this subsection use C_1 (no spatial) symmetry.

In order to precisely characterize the $^1A_1$ tetrahedral state, all six N–N bonds must be treated equivalently. This can be accomplished by using correlated methods based on a single reference state or multireference correlated methods based, for example, on a 12 electron–12 orbital (the six N–N bonds and six corresponding antibonding orbitals) CAS reference space. On the other hand, the $^3A''$ state arises from the excitation from an N–N bonding orbital (the 4a″ orbital pictured in Figure 2) to an antibonding N–N orbital. Consequently, the N–N bonds are inequivalent in this state and the system distorts from T_d to C_s symmetry. This state is well described by single reference state methods.[22]

To describe the minimum energy crossing point, a characterization of both the $^1A'$ and $^3A''$ states is required. Ideally this description would be based on a 12 in 12 CAS treatment in order to obtain a proper description of the $^1A'$ state at tetrahedral nuclear configurations. Such a treatment is extremely costly owing to the large active space. Instead, in this work a compromise approach is used which permits simultaneous description of both the $^1A'$ and $^3A''$ states and produces only limited distortion from tetrahedral symmetry of the local minimum on the $^1A'$ surface. In this description the $^1A'$ potential energy surface is described in the CSF space consisting of all single and double excitations relative to three reference electron configurations

$$1a'^2...9a'^2 10a'^2\ 1a''^2...4a''^2 \qquad (2.9a)$$

$$1a'^2...9a'^2 11a'^2\ 1a''^2...4a''^2 \qquad (2.9b)$$

$$1a'^2...9a'^2 10a'1a'\ 1a''^2...4a''^2 \qquad (2.9c)$$

Table II. N_4: Energies and Geometries of Minima Obtained from SDCI Wave Functions[a]

structure	MIN($^1A_1$)[b]	MIN($^3A''$)[c]	MEX($^3A''$–$^1A'$)
$R(N^1–N^2)$	1.435	1.332	1.239
$R(N^1–N^3)$	1.431	1.554	1.452
$R(N^2–N^3)$	1.431	2.333	2.479
$R(N^3–N^{3\prime})$	1.430	1.192	1.245
$E(^1A_1)$	−218.151 512		−218.106 322
$E(^3A'')$		−218.138 446	−218.106 323
ΔE	0	8.2	28.2

[a] Distances in angstroms, total energies in atomic units, $\Delta E \equiv E - E[\mathrm{MIN}(^1A_1)]$ in kcal/mol. For comparison $r_e[N_2(X^1\Sigma_g^+)] = 1.09768$ Å, $r_e[N_2(A^3\Sigma_u^+)] = 1.2826$ Å, $r_e[N_2(B^3\Pi_g)] = 1.2126$ Å (from ref 57). [b] $R(N^i–N^j) = 1.472$ Å (from ref 22) using CCSD(T) method, and $R(N^i–N^j) = 1.476$ Å (from ref 23), using MBPT(2) method. [c] $R(N^1–N^2) = 1.363$ Å, $R(N^1–N^3) = 1.514$ Å, $R(N^2–N^3) = 2.324$ Å, $R(N^3–N^{3\prime}) = 1.227$ Å using UMP2 method, and $\Delta E = 12.7$ kcal/mol using CPF method (from ref 22).

while the $^3A''$ potential energy surface is described in the CSF space consisting of all single and double excitations relative to the single reference electron configuration

$$1a'^2...9a'^2 10a'^2 11a'\ 1a''^2...3a''^2 4a'' \qquad (2.10)$$

In these spaces the four orbitals corresponding to the nitrogen 1s orbitals were held doubly occupied and the corresponding correlating molecular orbitals truncated. The molecular orbitals were determined using a SA-MCSCF procedure based on electron configurations 2.9 and 2.10 in which one $^1A'$ and one $^3A''$ state were averaged with equal weights. A double zeta polarization basis was used so that the dimension of the CSF spaces in question are (206 258; 410 646) for the $^1A'$ space and (211 212; 420 715) for the $^3A''$ space in (C_s; C_1) symmetry.

The reference configurations 2.9 and 2.10 were selected on the basis of preliminary, C_s symmetry, approximate second-order CI calculations based on the electron distribution $(1a'–8a',1a''–2a'')^{20}$ $\{9a'–12a',3a''–6a''\}^8$ using the DZP basis. The molecular orbitals for these calculations were determined from a SA-MCSCF procedure based on this active space in which one $^1A'$ and one $^3A''$ state were averaged with equal weights.

Table II reports the solution of eq 2.1, denoted MEX($^3A''$–$^1A'$), and compares it with the equilibrium structure for the $^1A'$ state, MIN($^1A'$) and for the $^3A''$ state MIN($^3A''$) obtained at the same level of treatment. As above, the energies reported in Table II illustrate the gratifying result that our algorithm for solving eq 2.1 routinely produces energies which are degenerate to less than 2×10^{-6} au. For these calculations the $\mathbf{W}^{JI}$ matrix in eq 2.1 was determined by centered difference differentiation using eq 2.4b. The geometrical data in Table II assume the C_s nuclear arrangement given in Figure 2. Both the MIN($^3A''$) and MEX($^3A''$–$^1A'$) structures have only this C_s symmetry. MIN($^1A'$), however, has approximate T_d symmetry, with the small distortion from the tetrahedral N_4 structure attributable to the reasons discussed above. Table II also compares the equilibrium structures obtained in the present work with those of Lee and Rice and those of Lauderdale et al. Agreement between the structures determined here and those reported previously is quite satisfactory. Our estimate of $\Delta E_{ST} \equiv E[\mathrm{MIN}(^3A')] - E[\mathrm{MIN}(^1A_1)] = 8.2(12.7)$ kcal/mol is in satisfactory accord with the result of Lee and Rice given parenthetically. This study thus confirms the existence of the low-lying triplet state. The comparisons presented with previous work serve to support the reliability of the present treatment.

From Table II we find that at the (C_s) minimum energy crossing point $\Delta E \equiv E[\mathrm{MEX}(^3A''–^1A')] - E[\mathrm{MIN}(^1A_1)] = 28.1$ kcal/mol. On the basis of the computed ΔE, the lowest-lying vibrational states are not expected to be significantly predissociated. However, the barrier to spin-forbidden predissociation is approximately half

(51) Berman, M. R.; Lin, M. C. *J. Phys. Chem.* **1983**, *87*, 3933.
(52) Dean, A. J.; Hanson, R. K.; Bowman, C. T. 23rd Symposium (International) on Combustion; The Combustion Institute: Pittsburgh, PA, 1990.
(53) Manaa, R.; Yarkony, D. R. *J. Chem. Phys.* **1991**, *95*, 1808.
(54) Manaa, M. R.; Yarkony, D. R. *Chem. Phys. Lett.* **1992**, *188*, 352.
(55) Dixon, D. A.; Komornicki, A.; Kraemer, W. P. *J. Chem. Phys.* **1984**, *81*, 3603.
(56) Woods, R. C.; Dixon, T. A.; Saykally, R. J.; Szanto, P. G. *Phys. Rev. Lett.* **1975**, *35*, 1269.
(57) Huber, K. P.; Herzberg, G. *Molecular Spectra and Molecular Structure. IV. Constants of Diatomic Molecules*; Van Nostrand Reinhold: New York, 1979.

that for the spin-allowed process. Thus consideration of this decay mechanism is essential to any realistic treatment of the lifetime of tetrahedral N_4.

Again a qualitative understanding of the processes associated with the singlet–triplet intersystem crossing at the minimum energy crossing can be obtained by examining the geometrical arrangement, and the topology of the potential energy surfaces, at this point. The structure corresponding to $MEX(^3A''-^1A')$ is qualitatively similar to that corresponding to $MIN(^3A'')$. For $MEX(^3A''-^1A')$ [and $MIN(^3A'')$], $R(N^1-N^2) \sim R(N^3-N^{3'}) \ll R(N^2-N^3) = R(N^2-N^{3'})$. While the short bond distances are comparable to the N–N distances of bound N_2 triplet states, $R(N^2-N^3)$ is appreciably longer than such bond lengths. For comparison, the equilibrium bond distances of $r_e[N_2(X^1\Sigma_g^+)]$, $r_e[N_2(A^3\Sigma_u^+)]$, and $r_e[N_2(B^3\Pi_g]$ are provided in Table II. An analysis of the energy gradients at $MEX(^3A''-^1A')$ shows that the "downhill" motion on the $^3A''$ potential energy surface decreases $R(N^3-N^3)$, tending to form a short N_2 bond, but increases all other bond distances. On the $^1A'$ potential energy surface the downhill direction increases $R(N^3-N^{3'})$ but decreases all other bond distances, a motion which is in the direction of the equilibrium geometry of tetrahedral N_4. These observations suggest that the intersystem crossing $^1A' \rightarrow {}^3A''$ is accompanied by the breaking of the N^2–N^3 and N^2–$N^{3'}$ bonds and ultimately results in the formation of two N_2 moieties. However, at $MEX(^3A''-^1A')$ the triplet wave function does not correspond to two incipient N_2 moieties. Thus a more detailed analysis of the $^3A''$ potential energy surface will be required to quantify the evolution of this system following intersystem crossing.

The spin–orbit interactions $H_\perp^{so}$ and $H_\parallel^{so}$ were determined at $MEX(^3A''-^1A')$ using the DZP basis and were found to be, $H_\perp^{so} = 18.8\ cm^{-1}$ and $H_\parallel^{so} = 34.8\ cm^{-1}$. These interactions are smaller than those obtained for CH_3O^+. However, using eq 2.8 in a manner analogous to that noted above, it is found that for vibrational levels above the minimum energy crossing this interaction is sufficient to produce an intersystem crossing in 10000 vibrational periods. As above, the determination of decay rates for predissociated vibrational levels requires a more complete analysis of the decay process.

Following the intersystem crossing, the N_4 moiety is on an excited potential energy surface. Thus additional crossings with the ground state singlet surface are possible as the system evolves into the product channel. However, as discussed above, in general the probability for a *single pass* intersystem crossing is small. Thus in the absence of the locally bound intermediates discussed at the end of subsection II.C, these additional crossings can be expected to be of secondary importance in the dynamics of the radiationless decay.

III. Summary and Conclusions

A Lagrange–Newton procedure[3] which uses analytic energy gradients to directly determine the minimum energy point on the spin-allowed crossing hypersurface of two states of different spin multiplicity has been used to examine the feasibility of spin-forbidden radiationless decay of a bound electronic state. The approach, which is of general utility, considers the energetics, geometrical arrangement, and character of the electronic wave functions at the minimum energy point on the multidimensional crossing hypersurface. These properties yield valuable mechanistic insights into this class of reactions, providing information concerning the feasibility of radiationless decay and the likely decomposition products.

This approach was used to study the radiationless decay of tetrahedral N_4, $N_4(^1A_1) \rightarrow N_4(^3A'') \rightarrow N_2(X^1\Sigma_g^+) + N_2(A^3\Sigma_u^-)$ and of the methoxy cation, $CH_3O^+(^3A_2) \rightarrow CH_3O^+(^1A') \rightarrow HCO^+(X^1\Sigma^+) + H_2(X^1\Sigma_g^+)$, two systems for which spin-forbidden decay has recently been postulated.[9,22] These systems were characterized using large scale multireference CI wave functions ranging in size from ~200000 to ~2500000 configuration state functions.

For the methoxy cation it is shown that the indicated reaction is a viable decomposition pathway. The barrier for this process, $\Delta E \equiv E[MEX(^3A''-^1A')] - E[MIN(^3A_2)]$, is only 15.4 kcal/mol. For tetrahedral N_4 the spin-forbidden decay channel has a barrier $\Delta E \equiv E[MEX(^3A''-^1A')] - E[MIN(^1A_1)]$ of approximately 28 kcal/mol. Thus the lowest-lying vibrational levels of this system are not expected to be significantly predissociated by this mechanism. However, the barrier for this process is approximately half the barrier for the spin-allowed decay channel that has been reported previously as approximately 61 kcal/mol.[22] Thus consideration of this decay mechanism is essential to any realistic treatment of the lifetime of tetrahedral N_4.

Acknowledgment. The N_4 calculations reported in this work were supported by a grant from the Air Force Office of Scientific Research, Grant No. AFOSR 90-0051. The CH_3O^+ calculations reported in this work were supported by a grant from the Department of Energy, Grant No. DE-FG02-91ER14189. All calculations reported herein were performed on DRY's IBM RISC 6000/550 workstations.

Registry No. N_4, 12596-63-3; CH_3O^+, 58157-09-8; CD_3O^+, 141272-04-0.